Aalborg Universitet

AALBORG UNIVERSITY
DENMARK

Do Lumped-Parameter Models Provide the Correct Geometrical Damping?

Andersen, Lars

Publication date:
2007

Document Version
Publisher's PDF, also known as Version of record

Link to publication from Aalborg University

Citation for published version (APA):
Andersen, L. (2007). *Do Lumped-Parameter Models Provide the Correct Geometrical Damping?* Aalborg: Department of Civil Engineering, Aalborg University. DCE Technical Memorandum, No. 5

General rights
Copyright and moral rights for the publications made accessible in the public portal are retained by the authors and/or other copyright owners and it is a condition of accessing publications that users recognise and abide by the legal requirements associated with these rights.

? Users may download and print one copy of any publication from the public portal for the purpose of private study or research.
? You may not further distribute the material or use it for any profit-making activity or commercial gain
? You may freely distribute the URL identifying the publication in the public portal ?

Take down policy
If you believe that this document breaches copyright please contact us at vbn@aub.aau.dk providing details, and we will remove access to the work immediately and investigate your claim.

Downloaded from vbn.aau.dk on: September 18, 2019

Do Lumped-Parameter Models Provide the Correct Geometrical Damping?

Lars Andersen

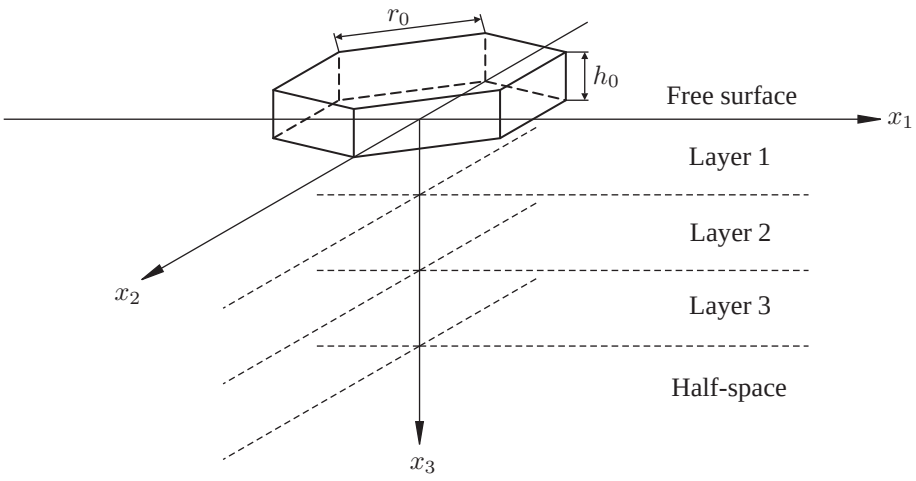

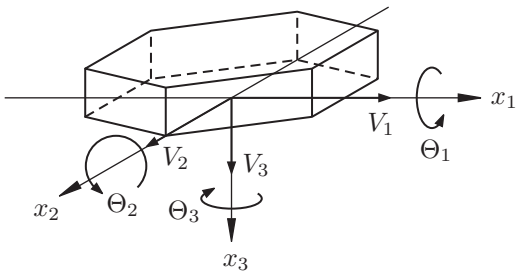

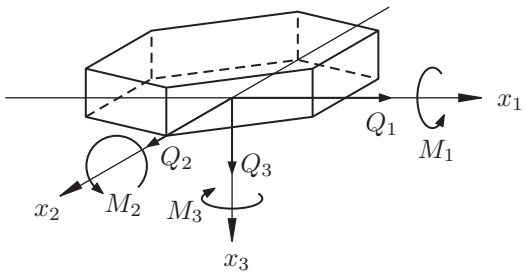

ISSN 1901-7278
DCE Technical Memorandum No. 5

AALBORG UNIVERSITY
Department of Civil Engineering

Aalborg University
Department of Civil Engineering
Water and Soil

DCE Technical Memorandum No. 5

Do Lumped-Parameter Models Provide the Correct Geometrical Damping?

by

Lars Andersen

March 2007

© Aalborg University

Scientific Publications at the Department of Civil Engineering

Technical Reports are published for timely dissemination of research results and scientific work carried out at the Department of Civil Engineering (DCE) at Aalborg University. This medium allows publication of more detailed explanations and results than typically allowed in scientific journals.

Technical Memoranda are produced to enable the preliminary dissemination of scientific work by the personnel of the DCE where such release is deemed to be appropriate. Documents of this kind may be incomplete or temporary versions of papers—or part of continuing work. This should be kept in mind when references are given to publications of this kind.

Contract Reports are produced to report scientific work carried out under contract. Publications of this kind contain confidential matter and are reserved for the sponsors and the DCE. Therefore, Contract Reports are generally not available for public circulation.

Lecture Notes contain material produced by the lecturers at the DCE for educational purposes. This may be scientific notes, lecture books, example problems or manuals for laboratory work, or computer programs developed at the DCE.

Theses are monograms or collections of papers published to report the scientific work carried out at the DCE to obtain a degree as either PhD or Doctor of Technology. The thesis is publicly available after the defence of the degree.

Latest News is published to enable rapid communication of information about scientific work carried out at the DCE. This includes the status of research projects, developments in the laboratories, information about collaborative work and recent research results.

Published 2007 by
Aalborg University
Department of Civil Engineering
Sohngaardsholmsvej 57,
DK-9000 Aalborg, Denmark

Printed in Denmark at Aalborg University

ISSN 1901-7278 DCE Technical Memorandum No. 5

Do lumped-parameter models provide the correct geometrical damping?

L. Andersen[†]

[†]*Department of Civil Engineering, Aalborg University, Aalborg, Denmark*

Abstract

This paper concerns the formulation of lumped-parameter models for rigid footings on homogenous or stratified soil. Such models only contain a few degrees of freedom, which makes them ideal for inclusion in aero-elastic codes for wind turbines and other models applied to fast evaluation of structural response in the time domain. However, the order of a lumped-parameter model must be sufficiently high to provide the correct dynamic stiffness of the ground. The aim of the present analysis is to examine the quality of low-order lumped-parameter models with respect to the prediction of the maximum response during excitation and the geometrical damping related to free vibrations of a hexagonal footing. The optimal order of a lumped-parameter model is determined for each degree of freedom, i.e. horizontal and vertical translation as well as torsion and rocking. In particular, the necessity of coupling between horizontal sliding and rocking is discussed.

Keywords: Foundations, soil dynamics, wave propagation, structural vibration.

1 Introduction

The dynamic response of engineering structures is highly dependent on the impedance of the foundation. The dynamic response of footings has been studied by several researchers. Torsional vibrations of a rigid circular footing were considered by Luco and Westmann [1], Veletsos and Nair [2], Novak and Sachs [3] and Aviles and Pérez-Rocha [4]. The vertical impedance of a flexible circular foundation on a homogeneous ground was examined by Krenk and Schmidt [5], while Yong et al. [6] considered a layered soil. Rocking and horizontal sliding of circular footings were considered by Veletsos and Wei [7], and by Luco [8]. Later, Wong and Luco [9] gave a solution to the impedance of rigid massless square foundations resting on layered viscoelastic soil, and Vrettos [10] studied the impedance of a rigid rectangular footing on a half-space with continuously increasing shear stiffness over depth. A further summary of the work concerning rocking and sliding of foundations was given by Bu and Lin [11].

Unfortunately, advanced numerical or analytical models describing the structure and the subsoil may be computationally inefficient—especially in the case of time-domain analyses. Alternatively, soil-structure interaction may be accounted for by fitting a lumped-parameter model (LPM) to the results of, for example, a finite-element (FE) model of the ground. In contrast to the original FE model, the LPM introduces few degrees of freedom in addition to those of the structure, thus leading to a significant reduction in the size of the global system of equations. This is particularly useful in parametric studies and lifetime analysis of structures.

The present paper concerns the calibration of consistent lumped-parameter models for rigid footings on a homogeneous or layered half-space with emphasis on three characteristics of the approximate solution: Firstly, the ability of an LPM to reproduce the maximum response of a structure subject to a transient load is examined; secondly, the damping of free vibrations is considered. Here, geometrical dissipation due to wave propagation into the subsoil accounts for the major part of the energy loss in the structure. Thirdly, the influence of coupling between horizontal sliding and rocking is examined, since the number of internal degrees of freedom in an LPM may be reduced significantly if such coupling may be disregarded.

Numerical studies show that the maximum response of the structure may be determined correctly by the application of an LPM with a few internal degrees of freedom, indicating that the dynamic stiffness of the footing is preserved. However, an accurate prediction of free vibrations cannot be achieved with low-order models, suggesting that geometrical dissipation is not well-represented. This leads to the conclusion that an LPM with several parameters is necessary to correctly predict the fatigue lifetime of structures subject to repeated transient loads. Finally, in the case of a footing on a homogeneous half-space, sliding–rocking coupling may be disregarded with little loss of accuracy. However, a correct prediction of the geometrical damping in stratified soil may only be achieved when the coupling is taken into consideration.

2 Model of the ground and footing

The foundation is modelled as a regular hexagonal rigid footing with the side length r_0, height h_0 and mass density ρ_0. This geometry is typical for offshore wind turbine foundations. As illustrated in Fig. 1, the centre of the soil–foundation interface coincides with the origin of the Cartesian coordinate system. The mass of the foundation and the corresponding mass moments of inertia with respect to the three coordinate axes then become:

$$M_0 = \rho_0 h_0 A_0, \quad \mathcal{J}_1 = \mathcal{J}_2 = \rho_0 h_0 \mathcal{I}_0 + \frac{1}{3}\rho_0 h_0^3 A_0, \quad \mathcal{J}_3 = 2\rho_0 h_0 \mathcal{I}_0, \tag{1a}$$

where A_0 is the area of the horizontal cross-section and I_0 is the corresponding geometrical moment of inertia,

$$A_0 = \frac{3\sqrt{3}}{2} r_0^2, \quad \mathcal{I}_0 = \frac{5\sqrt{3}}{16} r_0^4. \tag{1b}$$

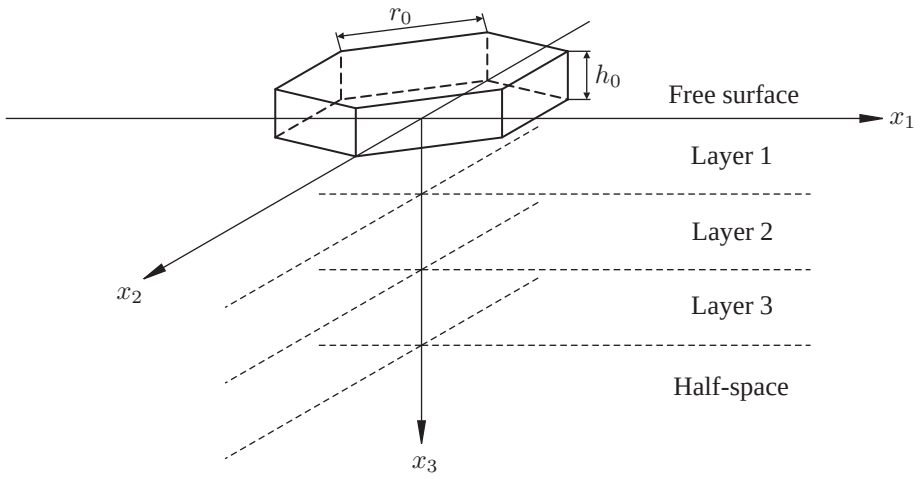

Figure 1: Hexagonal footing on a stratum with three layers over a half-space.

It is noted that $\mathcal{I}_0$ is invariant to rotation of the foundation around the x_3-axis. This property also applies to circular or quadratic foundations.

The ground consists of J horizontal layers over a homogeneous half-space (see Fig. 1). The soil in each layer and the underlying half-space is idealised as a linear viscoelastic, homogeneous and isotropic material defined by the mass density ρ^j, the P-wave velocity c_P^j and the S-wave velocity c_S^j, $j = 1, 2, \ldots, J+1$ (material $J+1$ refers to the half-space). Hysteretic damping with the loss factor η^j is assumed, knowing well that this provides a non-causal response of the ground. However, for small values of η^j, the error is acceptable [12, 13]. The material damping model is further discussed below. All interfaces, including the soil–foundation interface, are rough, i.e. welded contact is assumed.

The surface of the ground is defined by $x_3 = 0$ (see Fig. 1). In the time domain, and in terms of Cartesian coordinates, the components of the surface displacement and traction are denoted $u_i(x_1, x_2, t)$ and $p_i(x_1, x_2, t)$, respectively, where $i = 1, 2, 3$. Further, g_{ij} represents the Green's function providing the displacement in direction i at the observation point $(x_1, x_2, 0)$ and time t due to a unit force applied in direction j at the source point $(y_1, y_2, 0)$ and time τ. The total displacement at the observation point then becomes

$$u_i(x_1, x_2, t) = \int_{-\infty}^{t} \int_{-\infty}^{\infty} \int_{-\infty}^{\infty} g_{ij}(x_1 - y_1, x_2 - y_2, t - \tau) p_j(y_1, y_2, \tau) \, \mathrm{d}y_1 \mathrm{d}y_2 \mathrm{d}\tau, \quad (2)$$

where summation is applied over repeated indices. In Eq. (2) it has been utilised that the response is linear and that all interfaces are horizontal. This involves that the Green's function is invariant to spatial and temporal translation and, in addition to this, a triple Fourier transformation may be carried out with regard to time and the two horizontal coordinates. This reduces the convolution (2) to a set of algebraic equations,

$$\bar{U}_i(k_1, k_2, \omega) = \bar{G}_{ij}(k_1, k_2, \omega) \bar{P}_j(k_1, k_2, \omega), \quad (3)$$

which must be solved for each combination of the circular frequency ω and the horizontal wavenumbers k_1 and k_2. Whereas the Green's function g_{ij} cannot be established analytically for the stratified half-space, a closed-form solution for its triple Fourier transform $\bar{G}_{ij}(k_1, k_2, \omega)$ has been presented by, for example, Sheng et al. [14].

The surface displacements $U_i(x_1, x_2, \omega)$ in the frequency domain and spatial coordinates is established by inverse Fourier transformation of $\bar{U}_i(k_1, k_2, \omega)$ with respect to the horizontal wavenumbers. This operation becomes particularly simple when performed in polar coordinates [15], which requires the traction $P_j(x_1, x_2, \omega)$ to be symmetric around the x_3-axis. However, the surface displacements due to any distribution of the surface traction can be obtained, for example, by the mesh-free method proposed by Andersen and Clausen [16]. This is further discussed in Subsection 2.2.

2.1 Impedance of rigid foundations

A rigid footing has three translational and three rotational degrees of freedom as illustrated in Fig. 2. In the frequency domain, these are related to the complex amplitudes of the corresponding forces and moments as

$$\mathbf{C}(\omega)\mathbf{Z}(\omega) = \mathbf{F}(\omega), \tag{4a}$$

$$\mathbf{Z}(\omega) = \begin{bmatrix} V_1 & V_2 & V_3 & \Theta_1 & \Theta_2 & \Theta_3 \end{bmatrix}^T, \tag{4b}$$

$$\mathbf{F}(\omega) = \begin{bmatrix} Q_1 & Q_2 & Q_3 & M_1 & M_2 & M_3 \end{bmatrix}^T. \tag{4c}$$

In the general case, the impedance matrix $\mathbf{C}(\omega)$ is fully populated, i.e. all the rigid-body motions of the footing are interrelated. However, in the present case the footing is doubly-symmetric and rests on the surface of a horizontally layered stratum. Further, assuming that the stress resultants act at the centre of the soil–foundation interface, the torsional and vertical displacements are completely decoupled from the remaining degrees of freedom and the coupling between sliding in the x_1-direction

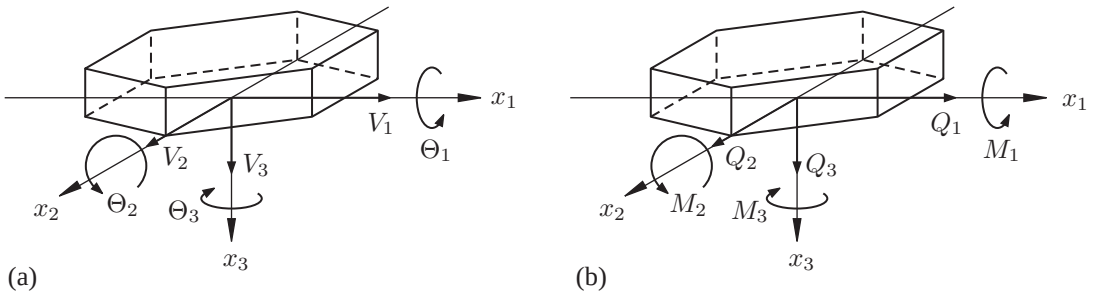

Figure 2: Degrees of freedom for a rigid surface footing: (a) displacements and rotations, and (b) forces and moments.

and rocking in the x_2-direction (and vice versa) vanishes, i.e.

$$\mathbf{C}(\omega) = \begin{bmatrix} C_{11} & 0 & 0 & 0 & -C_{24} & 0 \\ 0 & C_{22} & 0 & C_{24} & 0 & 0 \\ 0 & 0 & C_{33} & 0 & 0 & 0 \\ 0 & C_{24} & 0 & C_{44} & 0 & 0 \\ -C_{24} & 0 & 0 & 0 & C_{55} & 0 \\ 0 & 0 & 0 & 0 & 0 & C_{66} \end{bmatrix}. \tag{5}$$

The results $C_{11} = C_{22}$, $C_{44} = C_{55}$ and $C_{15} = -C_{24}$ follow from the fact that the geometrical moment of inertia, $\mathcal{I}_0$, of the hexagonal footing is the same for all horizontal axes through the centre of the soil–foundation interface.

2.2 Numerical procedure

The evaluation of the dynamic stiffness given by Eq. (5) has the following steps:

1. The displacement corresponding to each rigid-body mode is prescribed at L points distributed uniformly at the soil–foundation interface, cf. Fig. 3.
2. The Green's function matrix is evaluated in the wavenumber domain along the k_2-axis and $\bar{G}_{ij}(k_1, k_2, \omega)$ is evaluated by a simple coordinate transformation.
3. The wavenumber spectrum for a simple distributed load with unit magnitude and rotational symmetry around a point on the ground surface is computed.
4. The response at point l to a load centred at point m is calculated for all combinations of $l, m = 1, 2, ..., L$. This provides a flexibility matrix for the footing.
5. The unknown magnitudes of the loads applied at each of the points are computed. Integration of the stresses over the contact area provides the impedance.

As suggested by Andersen and Clausen [16], a "bell-shaped" load based on a double Gaussian distribution centred at the source point, m, is applied. The standard deviation in both horizontal coordinate directions is chosen as $r = r_0/\sqrt{4L}$.

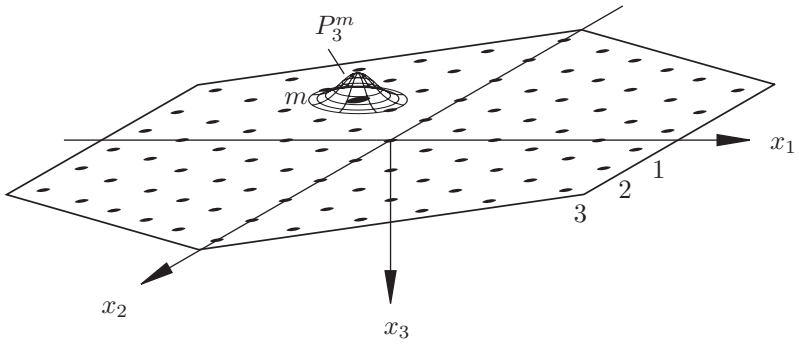

Figure 3: Discretization of the hexagonal footing. The vertical component of the "bell-shaped" load at point m is illustrated.

3 Lumped-parameter model of the footing

The components of the impedance matrix may be expressed as $C_{ij}(a_0) = K_{ij}S_{ij}(a_0)$ (no sum on i, j). Here, $K_{ij} = C_{ij}(0)$ denotes the static stiffness related to the interaction of the two degrees of freedom i and j, and $a_0 = \omega r_0/c_0$ is a non-dimensional frequency with r_0 and c_0 denoting the side length of the footing and a representative wave velocity in the ground, respectively.

For simplicity, the subscripts i and j are omitted in the following, e.g. $C(a_0) \sim C_{ij}(a_0)$. Then, as suggested by Wolf [17], the frequency-dependent stiffness coefficient $S(a_0)$ for component (i, j) of the impedance matrix is decomposed into a singular part, $S_s(a_0)$, and a regular part, $S_r(a_0)$,

$$C(a_0) = KS(a_0), \qquad S(a_0) = S_s(a_0) + S_r(a_0). \tag{6}$$

Here, K is the static stiffness component, and the singular part of the stiffness coefficient has the form

$$S_s(a_0) = k^\infty + \mathrm{i}a_0 c^\infty. \tag{7}$$

The two real constants k^∞ and c^∞ are selected so that $KS_s(a_0)$ provides the entire stiffness in the high-frequency limit $a_0 \to \infty$. For the rigid surface footing the term Kk^∞ vanishes, i.e. $k^\infty = 0$, and the complex stiffness in the high-frequency range becomes a pure mechanical impedance with

$$c_{11}^\infty = c_{22}^\infty = \frac{\rho c_S A_0}{K}, \quad c_{33}^\infty = \frac{\rho c_P A_0}{K}, \quad c_{44}^\infty = c_{55}^\infty = \frac{\rho c_P \mathcal{I}_0}{K}, \quad c_{66}^\infty = \frac{2\rho c_S \mathcal{I}_0}{K}, \tag{8}$$

where A_0 and $\mathcal{I}_0$ are given by Eq. (1b). The coupling terms $C_{15} = -C_{24}$ vanish in the high-frequency limit, i.e. there is no interaction between rocking and sliding.

The regular part $S_r(a_0)$ accounts for the remaining part of the dynamic stiffness and is obtained by fitting a rational filter to the results $S_r(a_0) = C(a_0)/K - S_s(a_0)$ obtained by the domain-transformation method, i.e.

$$S_r(a_0) \approx \hat{S}_r(\mathrm{i}a_0) = \frac{P(\mathrm{i}a_0)}{Q(\mathrm{i}a_0)}, \tag{9a}$$

where the numerator and denominator polynomials are given by

$$P(\mathrm{i}a_0) = 1 - k^\infty + p_1(\mathrm{i}a_0) + p_2(\mathrm{i}a_0)^2 + \ldots + p_{M-1}(\mathrm{i}a_0)^{M-1}, \tag{9b}$$

$$Q(\mathrm{i}a_0) = 1 + q_1(\mathrm{i}a_0) + q_2(\mathrm{i}a_0)^2 + \ldots + q_M(\mathrm{i}a_0)^M. \tag{9c}$$

The order of the filter, M, must be sufficiently high to ensure a reasonable fit to the "exact" solution provided by the domain-transformation method. However, to avoid wiggling of the approximation outside the fitted range of frequencies, M should not be too high. In this regard visual inspection of the rational approximation is useful. The coefficients, p_n ($n = 1, 2, \ldots, M-1$) and q_m ($m = 1, 2, \ldots, M$), of the numerator and denominator polynomials $P(\mathrm{i}a_0)$ and $Q(\mathrm{i}a_0)$ must all be real. Otherwise, the rational

filter cannot be interpreted in terms of temporal derivatives in the time domain and the solution is not physically sound.

The total approximation of $S(a_0)$ is found by an addition of Eqs. (7) and (9) as stated in Eq. (6). The approximation of $S(a_0)$ has two important characteristics:

- It is exact in the static limit, since $S(a_0) \approx S_s(a_0) + \hat{S}_r(\mathrm{i}a_0) \to 1$ for $a_0 \to 0$.
- It is exact in the high-frequency limit. Here, $S(a_0) \to S_s(a_0)$ for $a_0 \to \infty$, because $\hat{S}_r(\mathrm{i}a_0) \to 0$ for $a_0 \to \infty$.

Hence, the approximation is double-asymptotic. At intermediate frequencies, the quality of the fit depends on the order of the rational filter, and the overall accuracy depends on the discretization of the contact stresses at the soil–foundation interface.

3.1 Physical interpretation of a rational filter

The polynomial-fraction form (9) of the rational approximation is recast into partial-fraction form,

$$\hat{S}_r(\mathrm{i}a_0) = \sum_{m=1}^{M} \frac{A_m}{\mathrm{i}a_0 - s_m}, \tag{10}$$

where s_m, $m = 1, 2, \ldots, M$, are the poles of $\hat{S}_r(\mathrm{i}a_0)$, i.e. the roots of $Q(\mathrm{i}a_0)$, and A_m are the corresponding residues. These are generally complex, but as discussed above the coefficients q_m must all be real. Hence, any complex poles, s_m, and the corresponding residues, A_m, must appear as conjugate pairs. When two such terms are added together, a second-order term with real coefficients appears. Thus, with N complex conjugate pairs, the total approximation of the dynamic stiffness coefficient $S(a_0)$ can be written as

$$\hat{S}(\mathrm{i}a_0) = k^\infty + \mathrm{i}a_0 c^\infty + \sum_{n=1}^{N} \frac{\beta_{0n} + \beta_{1n}\mathrm{i}a_0}{\alpha_{0n} + \alpha_{1n}\mathrm{i}a_0 + (\mathrm{i}a_0)^2} + \sum_{n=N+1}^{M-N} \frac{A_n}{\mathrm{i}a_0 - s_n}, \tag{11}$$

where $2N \leq M$. The real coefficients α_{0n}, α_{1n}, β_{0n}, and β_{1n}, appearing in the second-order terms, are given by

$$\alpha_{0n} = \{s_n^{\Re}\}^2 + \{s_n^{\Im}\}^2, \qquad \alpha_{1n} = -2s_n^{\Re}, \tag{12a}$$

$$\beta_{0n} = -2A_n^{\Re}s_n^{\Re} + 2A_n^{\Im}s_n^{\Im}, \qquad \beta_{1n} = 2A_n^{\Re}, \tag{12b}$$

where $s_n^{\Re} = \Re(s_n)$ and $s_n^{\Im} = \Im(s_n)$ are the real and imaginary parts of the complex conjugate poles, respectively. Similarly, the real and imaginary parts of the complex conjugate residues are denoted by $A_n^{\Re} = \Re(A_n)$ and $A_n^{\Im} = \Im(A_n)$.

The total approximation of the dynamic stiffness given by Eq. (11) consists of three characteristic types of terms, namely a constant/linear term, $M - 2N$ first-order terms

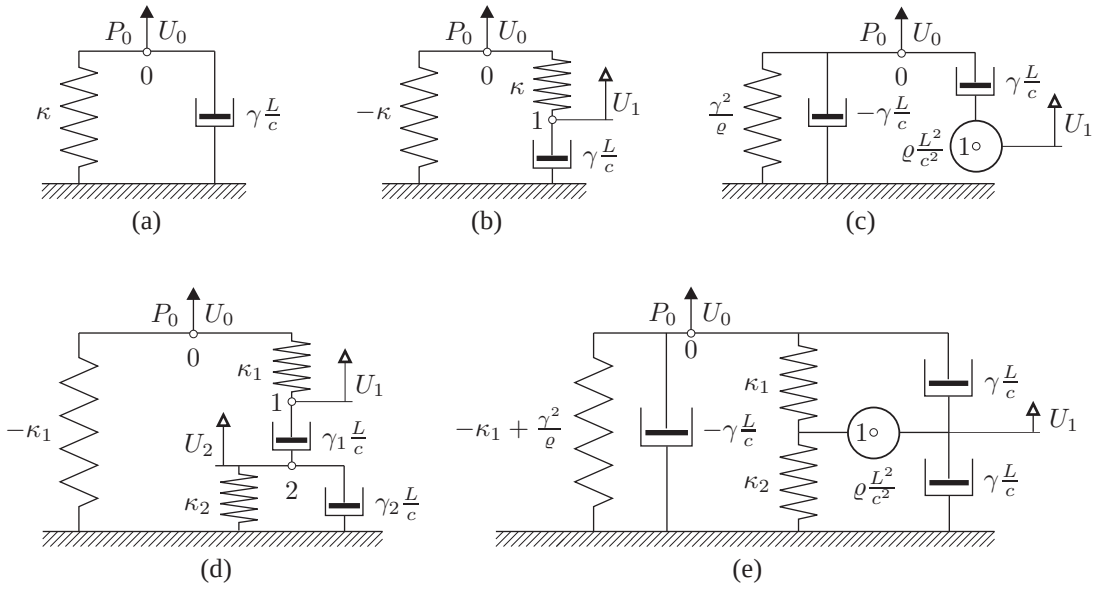

Figure 4: Discrete-element models: (a) Constant/linear term, (b) standard first-order term, (c) alternative first-order term ("monkey tail"), (d) standard second-order term (two internal degrees of freedom), and (e) alternative second-order term (one internal degree of freedom).

and N second-order terms. These are given as:

- Constant/linear term: $k^\infty + \mathrm{i}a_0 c^\infty$, (13a)
- First-order term: $\dfrac{A_n}{\mathrm{i}a_0 - s}$, (13b)
- Second-order term: $\dfrac{\beta_{0n} + \beta_{1n}\mathrm{i}a_0}{\alpha_{0n} + \alpha_{1n}\mathrm{i}a_0 + (\mathrm{i}a_0)^2}$. (13c)

Each of these expressions may be interpreted as the frequency-response function for a so-called discrete-element model as illustrated in Fig. 4. The spring and damping coefficients as well as the point masses in these models are uniquely defined in terms of the coefficients in Eq. (13). A detailed explanation may be found, for example, in the work by Wolf [17] or Liingaard [18]. Here, it shall only be noted that the optimal solution includes as many complex conjugate pairs as possible modelled by the alternative second-order system, cf. Fig. 4e, since this reduces the number of internal degrees of freedom in the resulting lumped-parameter model (LPM) to a minimum for a given order, M, of the rational approximation.

3.2 Some comments on the fitting of a rational filter

The rational approximation is obtained by curve-fitting of $\hat{S}_r(\mathrm{i}a_0)$ to the regular part of the dynamic stiffness, $S_r(a_0)$, by a weighted least-squares technique. In this process, a number of requirements must be met:

1. The response must be accurately described by the lumped-parameter model in the frequency range relevant for the physical problem being investigated.

2. The "exact" values of $S_r(a_0)$ are only computed (or measured) over a finite range of frequencies, $a_0 \in [0; a_{0\,\max}]$. Beyond this frequency range, the singular part of the dynamic stiffness, $S_s(a_0)$, should govern the response. Further, the values of $S_r(a_0)$ are typically only known at a number of discrete frequencies. The order of the filter should be sufficiently low to avoid wiggling with regard to both interpolation and extrapolation of the frequency response. In other words, no spikes are allowed in $\hat{S}(\mathrm{i}a_0)$ between two frequencies at which $S_r(a_0)$ has been determined, and no tips and dips should appear beyond $a_0 = a_{0\,\max}$.

3. In order to get a stable solution in the time domain, the poles of $\hat{S}_r(\mathrm{i}a_0)$ should all reside in the second and third quadrant of the complex plane, i.e. the real parts of the poles must all be negative. In iterative optimisation algorithms with a finite precision, this requirement should be adjusted to $s_m < -\varepsilon$, $m = 1, 2, \ldots, M$, where ε is a small number, e.g. 0.01.

To meet the two first requirements, experience shows that the order of the rational approximation is advantageously set to $M = 4 \sim 6$ for a footing on a homogeneous half-space and $M = 6 \sim 12$ for a footing over a stratified ground. Higher-order filters are not easily fitted, and lower-order approximations provide a poor match to the "exact" results. Further, in order to ensure a good fit of $\hat{S}_r(\mathrm{i}a_0)$ to $S_r(a_0)$ in the the low-frequency range $a_0 < 0.2 \sim 2$, a higher weight on the squared errors should be employed in the low-frequency range compared with the weights in the medium-to-high-frequency range.

Wolf [17] simply suggested to employ the weight $w = 10^3 \sim 10^5$ at low frequencies and unit weight at higher frequencies. This should lead to a good approximation in most cases. However, numerical experiments indicate that the fitting ability of the rational filter is highly sensitive to the choice of the weight function $w = w(a_0)$, and the guidelines provided by Wolf [17] are not useful in all situations. Hence, as an alternative, the following fairly general weight function is proposed:

$$w(a_0) = \frac{1}{(1 + (\varsigma_1 a_0)^{\varsigma_2})^{\varsigma_3}}. \tag{14}$$

The coefficients ς_1, ς_2 and ς_3 are heuristic parameters. Experience shows that values of about $\varsigma_1 = \varsigma_2 = \varsigma_3 = 2$ provide an adequate solution for most foundations in the low-frequency range $a_0 \in [0; 2]$. This recommendation is justified by the examples given in the following sections. For analyses involving high-frequency excitation, lower values of ς_1, ς_2 and ς_3 may have to be employed.

To meet the third requirement listed above, i.e. that all poles reside in the second and third quadrant of the complex plane, the representation of the rational approximation provided by Eq. (9) is inefficient with regard to the optimisation, or curve-fitting, process. Specifically, the choice of the polynomial coefficients q_j, $j = 1, 2, \ldots, m$, as

the optimisation variables is unsuitable, since the constraint that all poles of $\hat{S}_r(\mathrm{i}a_0)$ must have negative real parts is not easily incorporated in the optimisation problem. Therefore, instead of the form (9c), the denominator polynomial in the rational approximation is written as

$$Q(\mathrm{i}a_0) = \prod_{n=1}^{N} (\mathrm{i}a_0 - s_n)\,(\mathrm{i}a_0 - s_n^*) \cdot \prod_{n=N+1}^{M-N} (\mathrm{i}a_0 - s_n)\,. \tag{15}$$

In this representation, s_n, $n = 1, 2, \ldots, N$, are N complex roots of $Q(\mathrm{i}a_0)$ and s_n^*, $n = 1, 2, \ldots, N$, are their complex conjugates, whereas s_n, $n = N+1, N+2, \ldots, M-N$ are $M - 2N$ real roots of $Q(\mathrm{i}a_0)$.

Thus, in addition to the coefficients of the numerator polynomial $P(\mathrm{i}a_0)$, the variables in the optimisation problem are the real and imaginary parts $s_n^{\Re} = \Re(s_n)$ and $s_n^{\Im} = \Im(s_n)$ of the complex poles s_n, $n = 1, 2, \ldots, N$, and the real poles s_n, $n = N+1, N+2, \ldots, M-N$. The great advantage of the representation (15) is that the constraints on the poles are defined directly on each individual variable, whereas in the formulation with $Q(\mathrm{i}a_0)$ defined by Eq. (9c), the constraints are given on functionals of the variables. Hence, the solution is much more efficient and straightforward. However, Eq. (15) has two disadvantages when compared with Eq. (9c):

- The number of complex conjugate pairs has to be estimated. However, experience shows that as many of the roots as possible should appear as complex conjugates—e.g. $2N = M$ should be used if M is even. This provides a good fit in most situations and may, at the same time, generate the lumped-parameter model with fewest possible internal degrees of freedom given that the second-order discrete-element model shown in Fig. 4(e) is utilised.

- In the representation provided by Eq. (9c), the correct asymptotic behaviour is automatically ensured in the limit $\mathrm{i}a_0 \to 0$, i.e. the static case, since $q_0 = 1$. Unfortunately, in the representation given by Eq. (15), an additional equality constraint has to be implemented to ensure this behaviour. However, this condition is much easier implemented into an optimisation algorithm than the constraints which are necessary in the case of Eq. (9c) in order to prevent the real parts of the roots from being positive.

Finally, additional constraints are suggested which prevent the imaginary parts of the complex poles to become much (e.g. 10 times) greater than the real parts. If the real part of the complex pole s_m vanishes, i.e. $s_m^{\Re} = 0$, this results in a second order pole, $\{s_m^{\Im}\}^2$, which is real and positive. Evidently, this will lead to instability in the time domain. Since computer precision is finite, a real part of a certain size relatively to the imaginary part of the pole is necessary to ensure a stable solution. All the above-mentioned constraints have been implemented into a Fortran code based on the NLPQL optimisation algorithm [19].

4 A footing on a homogeneous half-space

Firstly, we consider a hexagonal footing on a homogeneous visco-elastic half-space. The footing has the side length $r_0 = 10$ m, the height $h_0 = 10$ m and the mass density $\rho_0 = 2000$ kg/m^3, and the mass and mass moments of inertia are computed by Eq. (1). The properties of the soil are $\rho^1 = 2000$ kg/m^3, $E^1 = 10^4$ kPa, $\nu^1 = 0.25$ and $\eta^1 = 0.03$. However, in the static limit, i.e. for $\omega \to 0$, the hysteretic damping model leads to a complex impedance in the frequency domain. By contrast, the lumped-parameter model provides a real impedance, since it is based on viscous dashpots. This discrepancy leads to numerical difficulties in the fitting procedure and to overcome this, the hysteretic damping model for the soil is replaced by a linear viscous model at low frequencies, in this case below 1 Hz.

In principle, the time-domain solution for the displacements and rotations of the rigid footing is found by inverse Fourier transformation, i.e.

$$v_i(t) = \frac{1}{2\pi}\int_{-\infty}^{\infty} V_i(\omega)\mathrm{e}^{\mathrm{i}\omega t}\mathrm{d}\omega, \quad \theta_i(t) = \frac{1}{2\pi}\int_{-\infty}^{\infty} \Theta_i(\omega)\mathrm{e}^{\mathrm{i}\omega t}\mathrm{d}\omega, \quad i = 1,2,3. \tag{16}$$

In the numerical computations, the frequency response spectrum is discretized and accordingly, the time-domain solution is found by a Fourier series.

4.1 Vertical and torsional motion

According to Eq. 5, the vertical motion $v_3(t)$ as well as the torsional motion $\theta_3(t)$ (see Fig. 2) are decoupled from the remaining degrees of freedom of the hexagonal footing. Thus, $v_3(t)$ and $\theta_3(t)$ may be fitted by independent lumped-parameter models. In the following, the quality of lumped-parameter models based on rational filters of different orders are tested for vertical and torsional excitation.

For the footing on the homogeneous half-space, rational filters of the order 2–6 are tested. Firstly, the impedance components are determined in the frequency-domain by the domain-transformation method presented in Section 2. The lumped-parameter models are then fitted by application of the procedure described in Section 3.2. The two components of the normalised impedance, S_{33} and S_{66}, are shown in Figs. 5 and 6 as functions of the physical frequency, f. It is noted that all the lumped-parameter models are based on second-order discrete-element models including a point mass, see Fig. 4(e). Hence, the LPM for each individual component of the impedance matrix, $\mathbf{C}(\omega)$, has 1, 2 or 3 internal degrees of freedom.

With reference to Fig. 5, a poor fit of the vertical impedance is obtained with $M = 2$ regarding the absolute value of S_{33} as well as the phase angle. A lumped-parameter model with $M = 4$ provides a much better fit in the low-frequency range. However, a sixth-order lumped-parameter model is required to obtain an accurate solution in the medium-frequency range, i.e. for frequencies between approximately 1.5 and 4 Hz. As expected, further analyses show that a slightly better match in the medium-frequency range is obtained with the weight-function coefficients $\varsigma_1 = 2$ and $\varsigma_2 = \varsigma_3 = 1$. However, this comes at the cost of a poorer match in the low-frequency range. Finally,

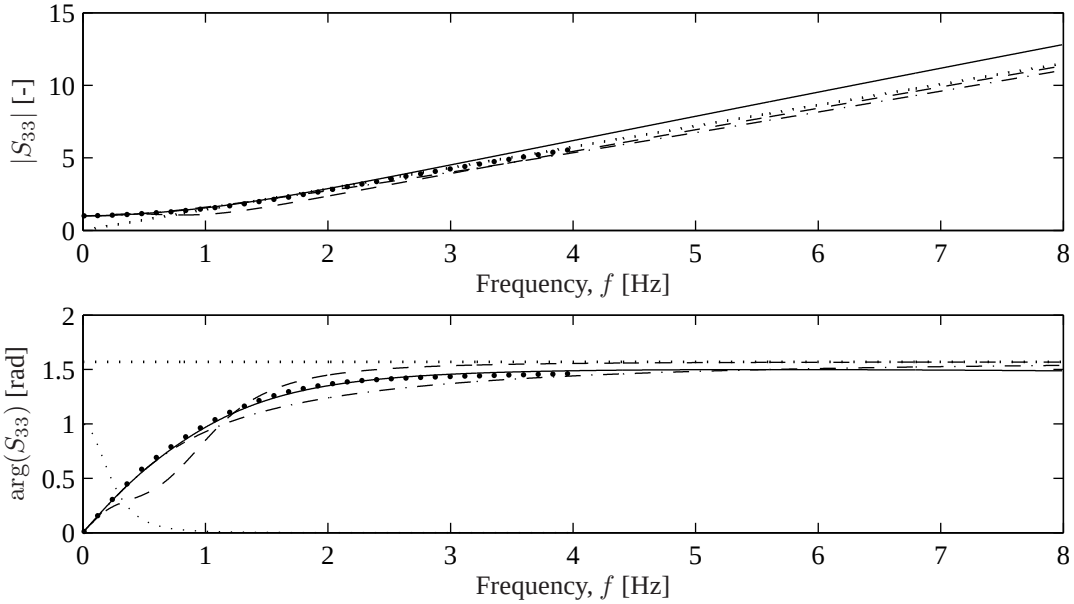

Figure 5: Dynamic stiffness coefficient, S_{33}, obtained by the domain-transformation model (the large dots) and lumped-parameter models with $M = 2$ (– –), $M = 4$ (– · – ·), and $M = 6$ (——). The thin dotted line (·····) indicates the weight function w (not in radians), and the thick dotted line (·····) indicates the high-frequency solution, i.e. the singular part of S_{33}.

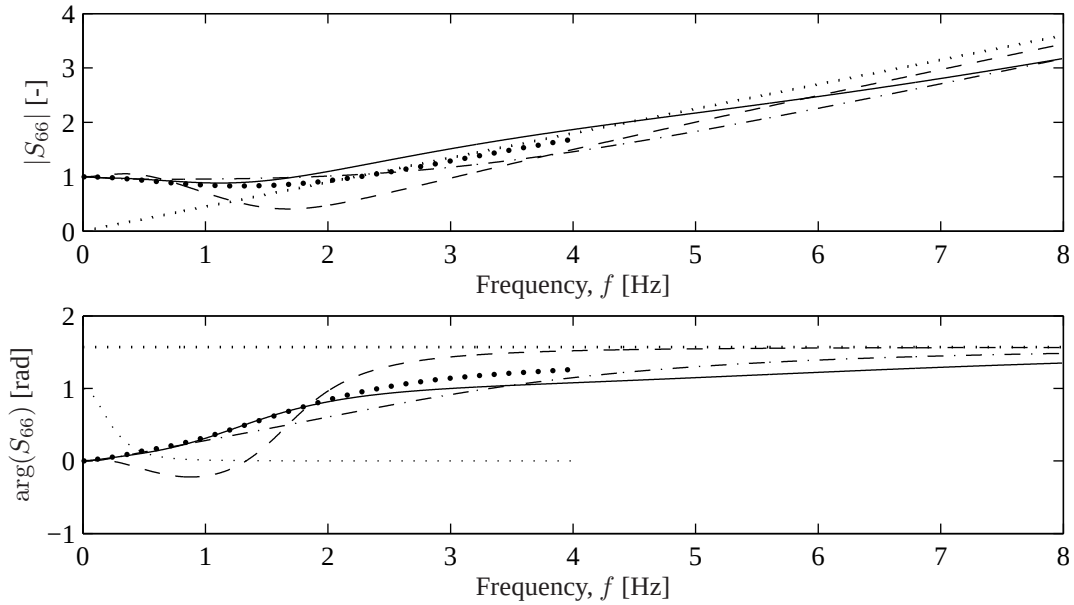

Figure 6: Dynamic stiffness coefficient, S_{66}, obtained by the domain-transformation model (the large dots) and lumped-parameter models with $M = 2$ (– –), $M = 4$ (– · – ·), and $M = 6$ (——). The thin dotted line (·····) indicates the weight function w (not in radians), and the thick dotted line (·····) indicates the high-frequency solution, i.e. the singular part of S_{66}.

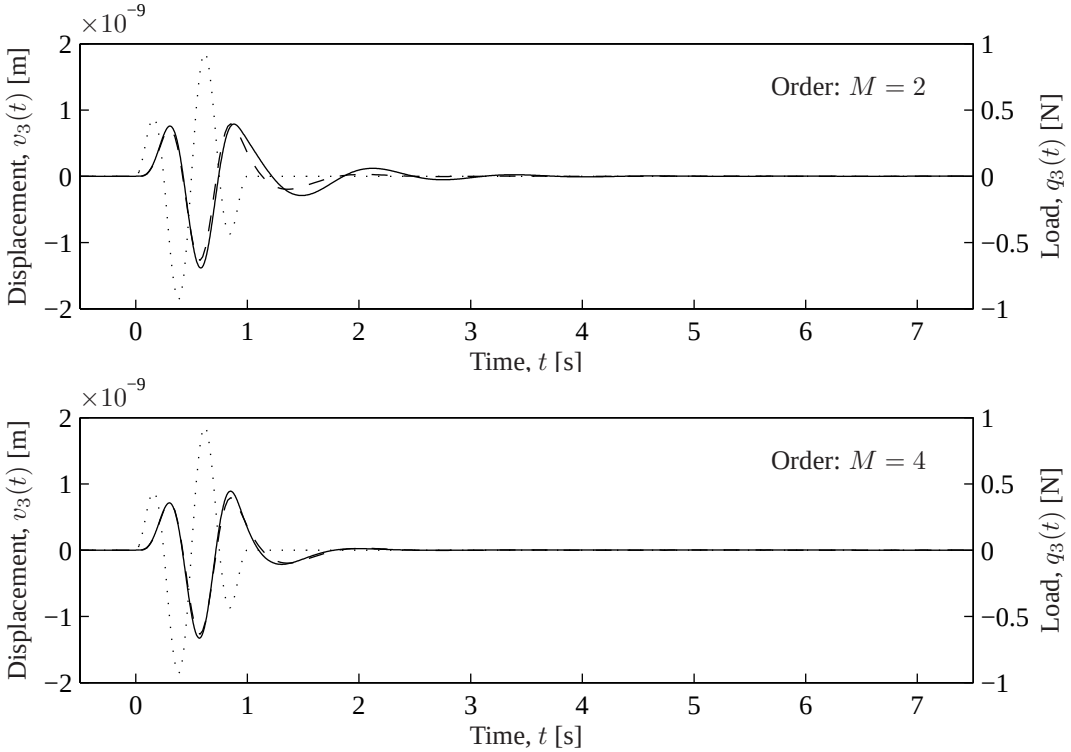

Figure 7: Response $v_3(t)$ obtained by inverse Fourier transformation (– –) and lumped-parameter model (——). The dots (·····) indicate the load time history.

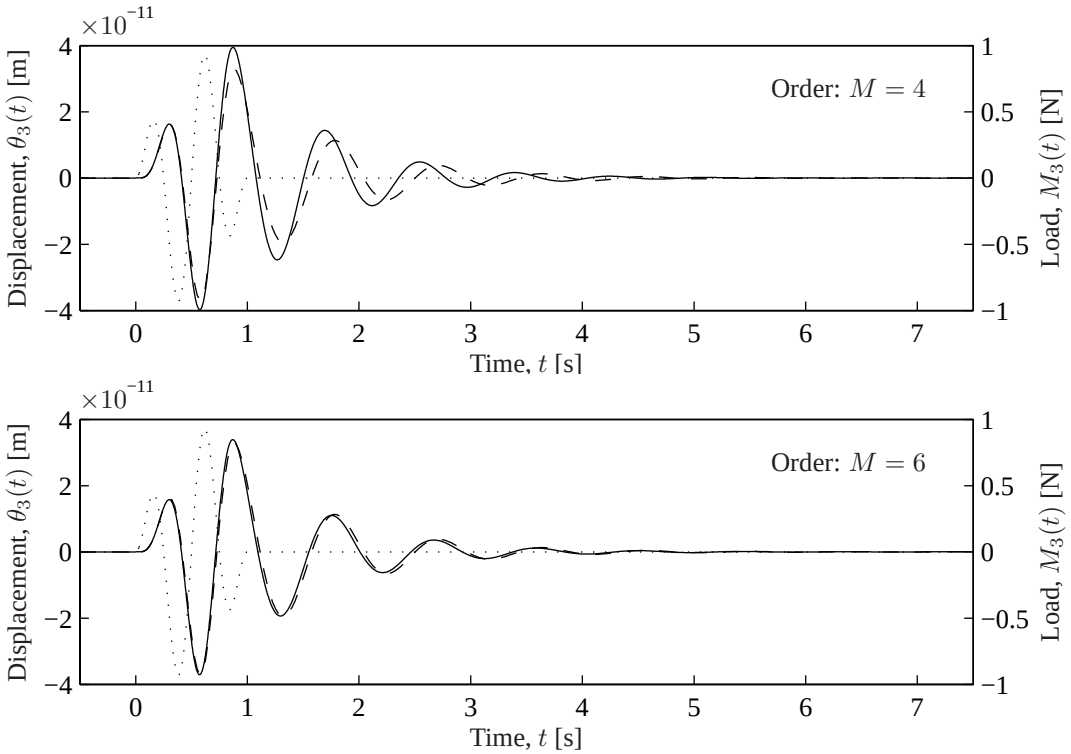

Figure 8: Response $\theta_3(t)$ obtained by inverse Fourier transformation (– –) and lumped-parameter model (——). The dots (·····) indicate the load time history.

it has been found that no improvement is achieved if first-order terms, e.g. the "monkey tail" illustrated in Fig. 4(c), are allowed in the rational-filter approximation.

Figure 6 shows the rational-filter approximations of S_{66}, i.e. the non-dimensional torsional impedance. Compared with the results for the vertical impedance, the overall quality of the fit is relatively poor. In particular the LPM with $M = 2$ provides a phase angle which is negative in the low frequency range. Actually, this means that the geometrical damping provided by the second-order LPM becomes negative for low-frequency excitation. Furthermore, the stiffness is generally under-predicted and as a consequence of this an LPM with $M = 2$ cannot be used for torsional vibrations of the surface footing. A significant improvement is achieved with $M = 4$, but even with $M = 6$ some discrepancies are observed between the results provide by the LPM and the rigorous model. Unfortunately, additional studies indicate that an LPM with $M = 8$ does not increase the accuracy beyond that of the sixth-order model.

Next, the dynamic soil–foundation interaction is studied in the time domain. In order to examine the transient response, a pulse load is applied in the form $p(t) = \sin(2\pi f_c t)\sin(0.5\pi f_c t)$ for $0 < t < 2/f_c$ and $p(t) = 0$ otherwise. In this analysis, $f_c = 2$ Hz is utilised, and the responses obtained with the lumped-parameter models of different orders are computed by application of the Newmark β-scheme [20]. Figure 7 shows the results of the analysis with $q_3(t) = p(t)$, whereas the results for $M_3(t) = p(t)$ are given in Fig. 8.

In the case of vertical excitation, Fig. 7 shows that even the LPM with $M = 2$ provides an acceptable match to the "exact" results achieved by inverse Fourier transformation of the frequency-domain solution. In particular, the maximum response occurring during the excitation is well described. However, a significant improvement in the description of the damping is obtained with $M = 4$. For torsional motion, the second-order LPM is invalid since it provides negative damping. Hence, the models with $M = 4$ and $M = 6$ are compared in Fig. 8. It is clearly demonstrated that the fourth-order LPM provides a poor representation of the torsional impedance, whereas an accurate prediction of the transient response is achieved with the sixth-order model.

4.2 Horizontal sliding and rocking

The next part of the analysis concerns the fitting of lumped-parameter models for the horizontal sliding and rocking motion of the surface footing, i.e. $v_2(t)$ and $\theta_1(t)$ (see Fig. 2). As indicated by Eqs. (4) and (5), these degrees of freedom are coupled via the impedance component C_{24}. Hence, two analyses are carried out. Firstly, the quality of lumped-parameter models based on rational filters of different orders are tested for horizontal and moment excitation. Secondly, the significance of coupling is investigated by a comparison of models with and without the coupling terms.

Similarly to the case for vertical and torsional motion, rational filters of the order 2–6 are tested. The three components of the normalised impedance, S_{22}, $S_{24} = S_{42}$ and S_{44}, are shown in Figs. 9 to 11 as functions of the physical frequency, f. Again, the lumped-parameter models are based on discrete-element model shown in Fig. 4(e),

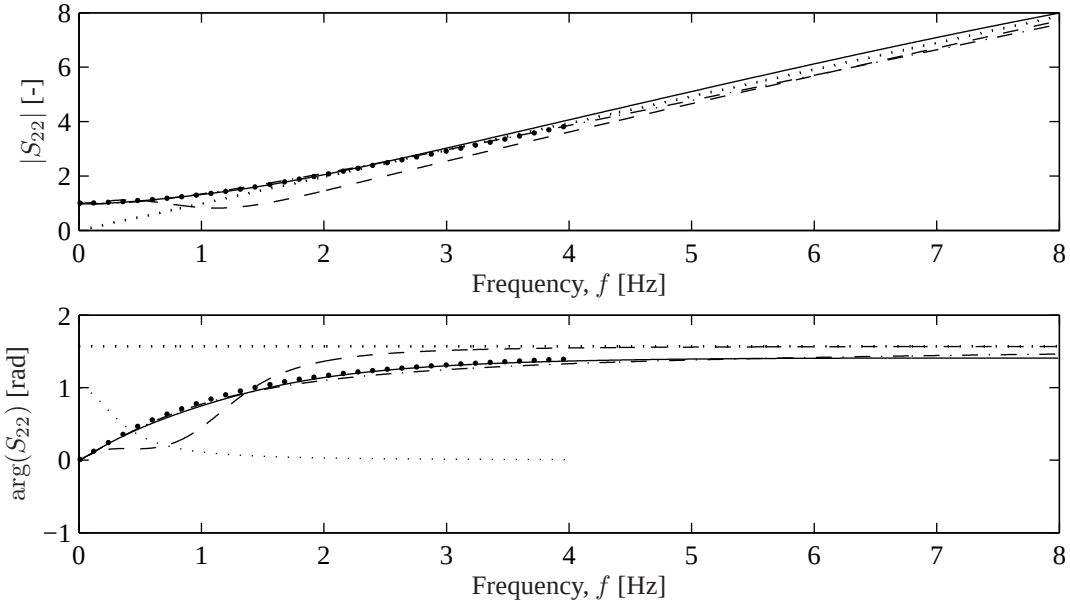

Figure 9: Dynamic stiffness coefficient, S_{22}, obtained by the domain-transformation model (the large dots) and lumped-parameter models with $M = 2$ (– –), $M = 4$ (– · – ·), and $M = 6$ (——). The thin dotted line (·····) indicates the weight function w (not in radians), and the thick dotted line (·····) indicates the high-frequency solution, i.e. the singular part of S_{22}.

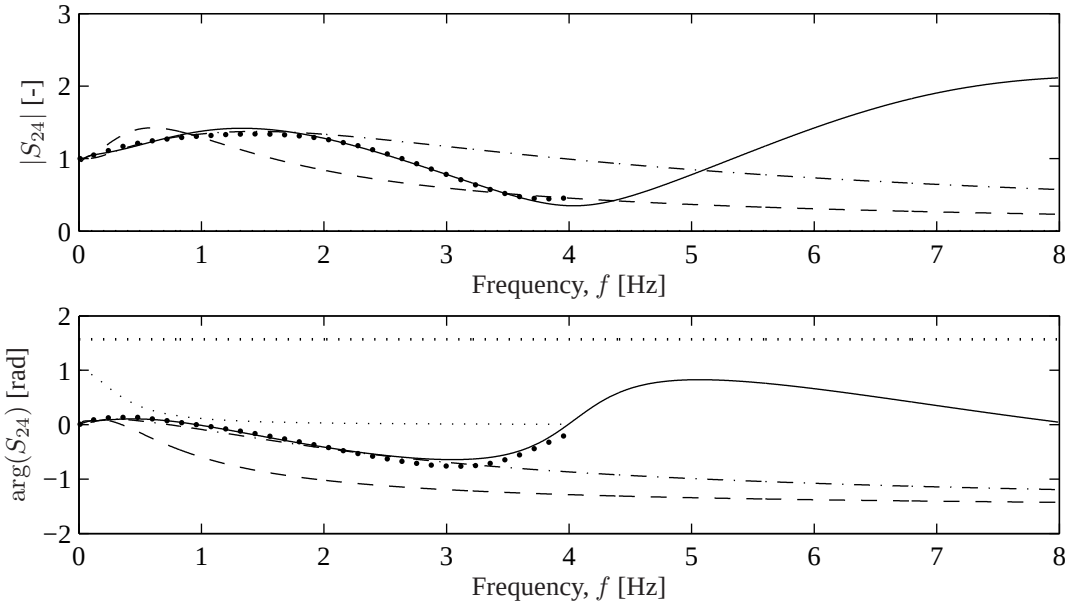

Figure 10: Dynamic stiffness coefficient, S_{24}, obtained by the domain-transformation model (the large dots) and lumped-parameter models with $M = 2$ (– –), $M = 4$ (– · – ·), and $M = 6$ (——). The thin dotted line (·····) indicates the weight function w (not in radians), and the thick dotted line (·····) indicates the high-frequency solution, i.e. the singular part of S_{24}.

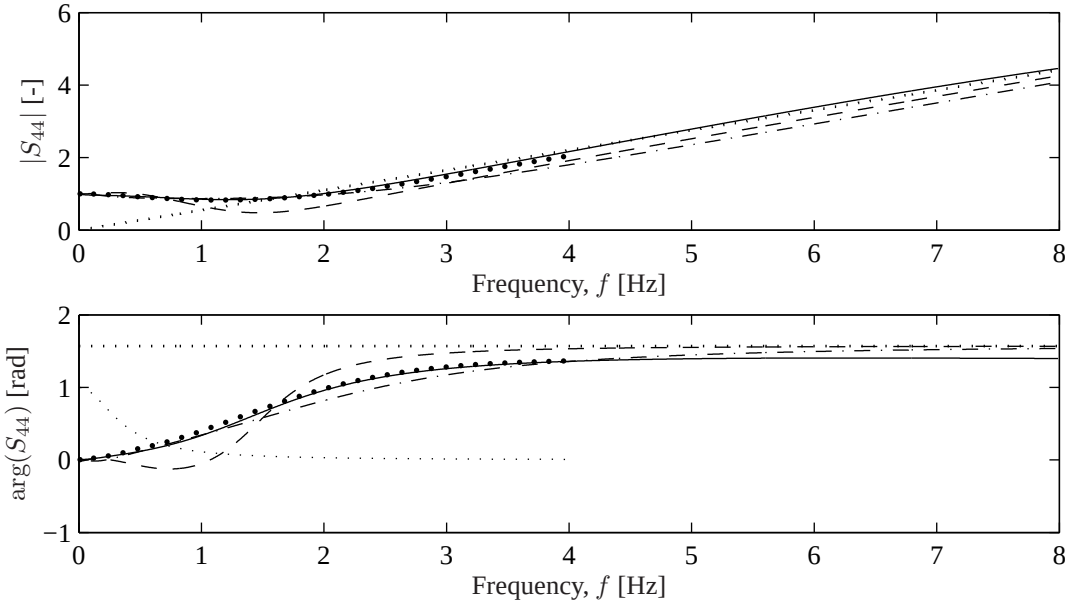

Figure 11: Dynamic stiffness coefficient, S_{44}, obtained by the domain-transformation model (the large dots) and lumped-parameter models with $M = 2$ (– –), $M = 4$ (– · – ·), and $M = 6$ (——). The thin dotted line (·····) indicates the weight function w (not in radians), and the thick dotted line (·····) indicates the high-frequency solution, i.e. the singular part of S_{44}.

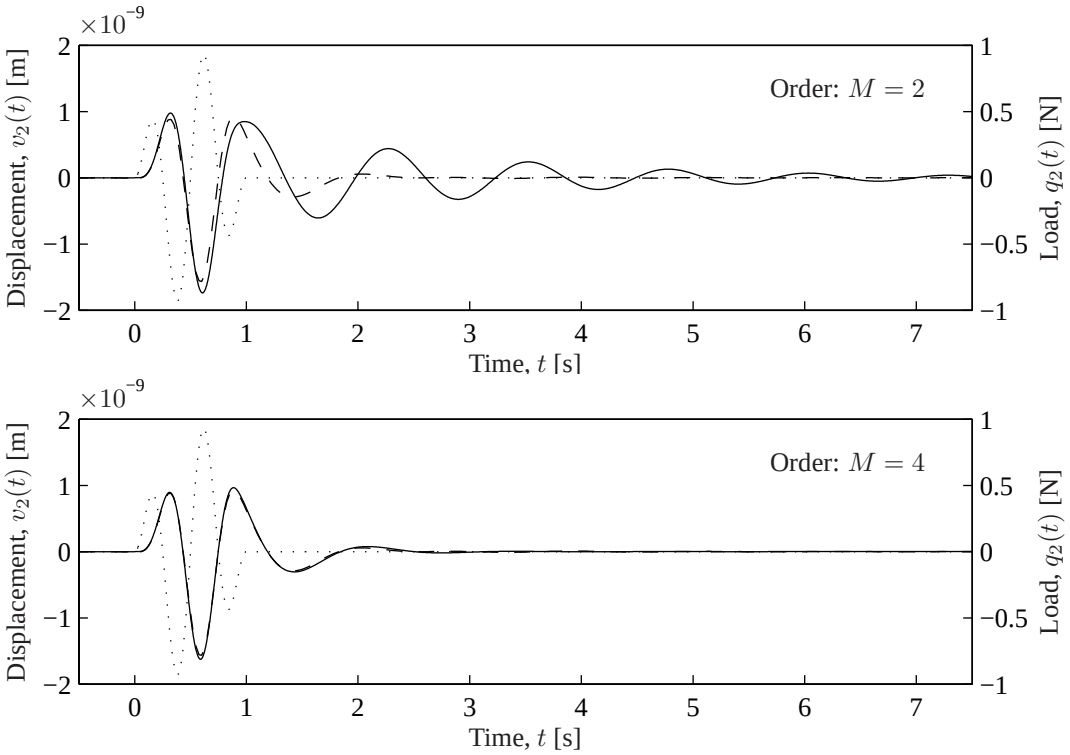

Figure 12: Response $v_2(t)$ obtained by inverse Fourier transformation (– –) and lumped-parameter model (——). The dots (·····) indicate the load time history.

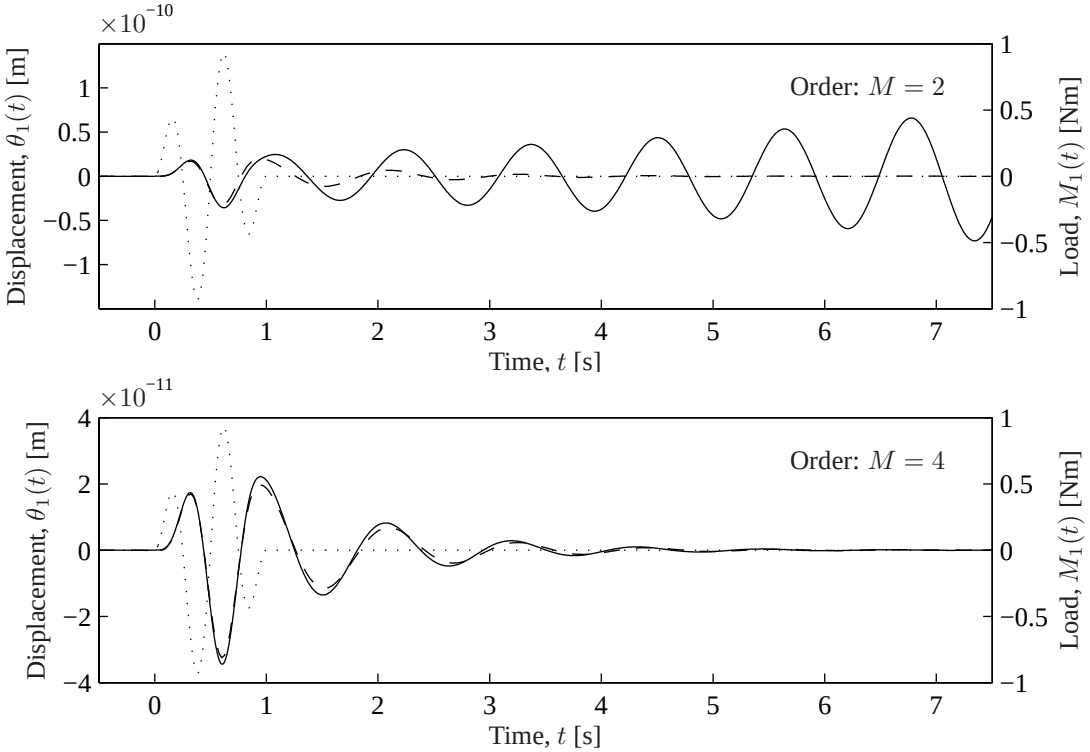

Figure 13: Response $\theta_1(t)$ obtained by inverse Fourier transformation (– –) and lumped-parameter model (——). The dots (·····) indicate the load time history.

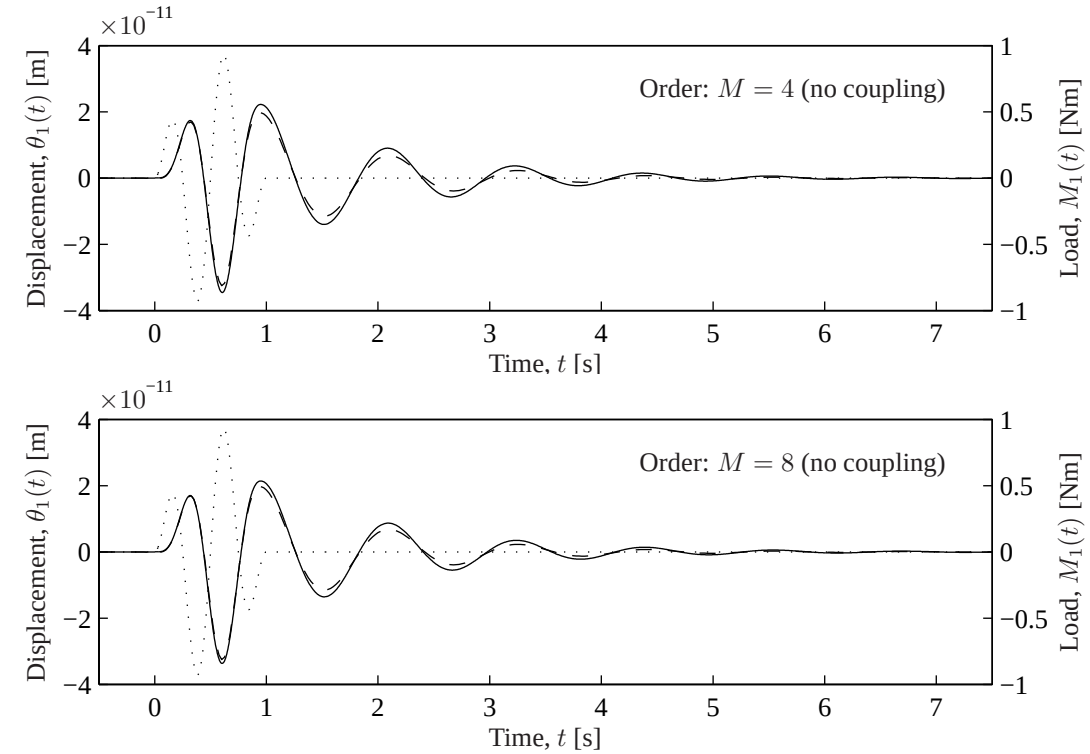

Figure 14: Response $\theta_1(t)$ obtained by inverse Fourier transformation (– –) and lumped-parameter model (——). The dots (·····) indicate the load time history.

which reduces the number of internal degrees of freedom to a minimum. Clearly, the lumped-parameter models with $M = 2$ provide a poor fit for all the components S_{22}, S_{24} and S_{44}. However, Figs. 9 and 11 show that an accurate solution is obtained for S_{22} and S_{44} when a fourth-order model is applied, and the inclusion of an additional internal degree of freedom, i.e. raising the order from $M = 4$ to $M = 6$, does not increase the accuracy significantly. On the other hand, for S_{24} an LPM with $M = 6$ is much more accurate than an LPM with $M = 4$ for frequencies $f > 3$ Hz, see Fig. 10.

Subsequently, the transient response to the previously defined pulse load with centre frequency $f_c = 2$ Hz is studied. Figure 12 shows the results of the analysis with $q_2(t) = p(t)$, and the results for $M_1(t) = p(t)$ are given in Fig. 13. Further, the results from an alternative analysis with no coupling of sliding and rocking are presented in Fig. 14. In Fig. 12 it is observed that the LPM with $M = 2$ provides a poor match to the results of the rigorous model. The maximum response occurring during the excitation is well described by the low-order LPM. However the damping is significantly underestimated by the LPM. Since the loss factor is small, this leads to the conclusion that the geometrical damping is not predicted with adequate accuracy. On the other hand, for $M = 4$ a good approximation is obtained with regard to both the maximum response and the geometrical damping. As suggested by Fig. 9, almost no further improvement is gained with $M = 6$. For the rocking produced by a moment applied to the rigid footing, the lumped-parameter model with $M = 2$ is useless. Here, the geometrical damping is apparently negative. However, the order $M = 4$ provides a fairly accurate solution (see Fig. 13) and again little improvement is achieved by raising the order to $M = 6$ (this result is not included in the figure).

Alternatively, Fig. 14 shows the result of the time-domain solution for a lumped-parameter model in which the coupling between sliding and rocking is disregarded. This model is interesting because the two coupling components S_{24} and S_{42} must be described by separate lumped-parameter models. Thus, the model with $M = 4$ in Fig. 14 has four less internal degrees of freedom than the corresponding model with $M = 4$ in Fig. 13. However, the two results are almost identical, i.e. the coupling is not pronounced for the footing on the homogeneous half-space. Hence, the sliding–rocking coupling may be disregarded without significant loss of accuracy. Increasing the order of the LPMs for S_{22} and S_{44} from 4 to 8 results in a model with the same number of internal degrees of freedom as the fourth-order model with coupling; but as indicated by Fig. 14, this does not improve the overall accuracy. Finally, Fig. 10 suggests that the coupling is more pronounced when a load with, for example, $f_c = 1.5$ or 3.5 Hz is applied. However, further analyses, whose results are not presented in this paper, indicate that this is not the case.

5 A footing on a layered half-space

Next, a stratified ground is considered. The soil consists of two layers over homogeneous half-space. Material properties and layer depths are given in Table 1. This may correspond to sand over a layer of undrained clay resting on limestone or bedrock.

Table 1: Material properties and layer depths for layered half-space.

Layer no.	h (m)	E (MPa)	ν	ρ (kg/m^3)	η
Layer 1	8	10	0.25	2000	0.03
Layer 2	16	5	0.49	2200	0.02
Half-space	∞	100	0.25	2500	0.01

The geometry and density of the footing are unchanged from the analysis of the homogeneous half-space.

5.1 Vertical and torsional motion

The non-dimensional vertical and torsional impedance components, i.e. S_{33} and S_{66}, are presented in Figs. 15 and 16 as functions of the physical frequency, f. In addition to the domain-transformation method results, the LPM approximations are shown for $M = 2$, $M = 6$ and $M = 10$. Clearly, low-order lumped-parameter models are not able to describe the local tips and dips in the frequency response of a footing on a layered ground. However, the LPM with $M = 10$ provides a good approximation of the vertical and torsional impedances for frequencies $f < 2$ Hz. It is worthwhile to note that the lumped-parameter models of the footing on the layered ground are actually more accurate than the models of the footing on the homogeneous ground. This follows by a comparison of Figs. 15 and 16 with Figs. 5 and 6.

The time-domain solutions for an applied vertical force, $q_3(t)$, or torsional moment, $M_3(t)$, are plotted in Fig. 17 and Fig. 18, respectively. Evidently, the lumped-parameter model with $M = 6$ provides an almost exact match to the solution obtained by inverse Fourier transformation—in particular in the case of vertical motion. However, in the case of torsional motion (see Fig. 18), the model with $M = 10$ is significantly better at describing the free vibration after the end of the excitation.

5.2 Horizontal sliding and rocking

The non-dimensional impedance components S_{22}, $S_{24} = S_{42}$ and S_{44} are shown in Figs. 19 to 21 as functions of the physical frequency, f. Again, the LPM approximations with $M = 2$, $M = 6$ and $M = 10$ are illustrated, and the low-order lumped-parameter models are found to be unable to describe the local variations in the frequency response. The LPM with $M = 10$ provides an acceptable approximation of the sliding, the coupling and the rocking impedances for frequencies $f < 2$ Hz, but generally the match is not as good as in the case of vertical and torsional motion.

The transient response to a horizontal force, $q_2(t)$, or rocking moment, $M_1(t)$, are shown in Figs. 22 and 23. Again, the LPM with $M = 6$ provides an almost exact match to the solution obtained by inverse Fourier transformation. However, the model with $M = 10$ is significantly better at describing the free vibration after the end of the excitation. This is the case for the sliding, $v_2(t)$, as well as the rotation, $\theta_1(t)$.

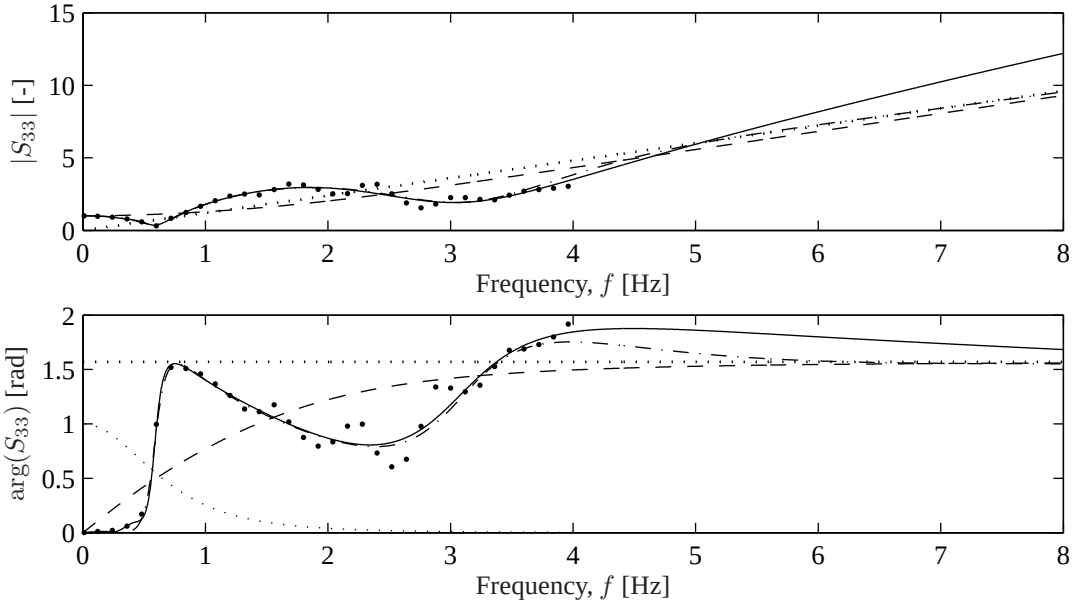

Figure 15: Dynamic stiffness coefficient, S_{33}, obtained by the domain-transformation model (the large dots) and lumped-parameter models with $M = 2$ (– –), $M = 6$ (– · – ·), and $M = 10$ (——). The thin dotted line (·····) indicates the weight function w (not in radians), and the thick dotted line (·····) indicates the high-frequency solution, i.e. the singular part of S_{33}.

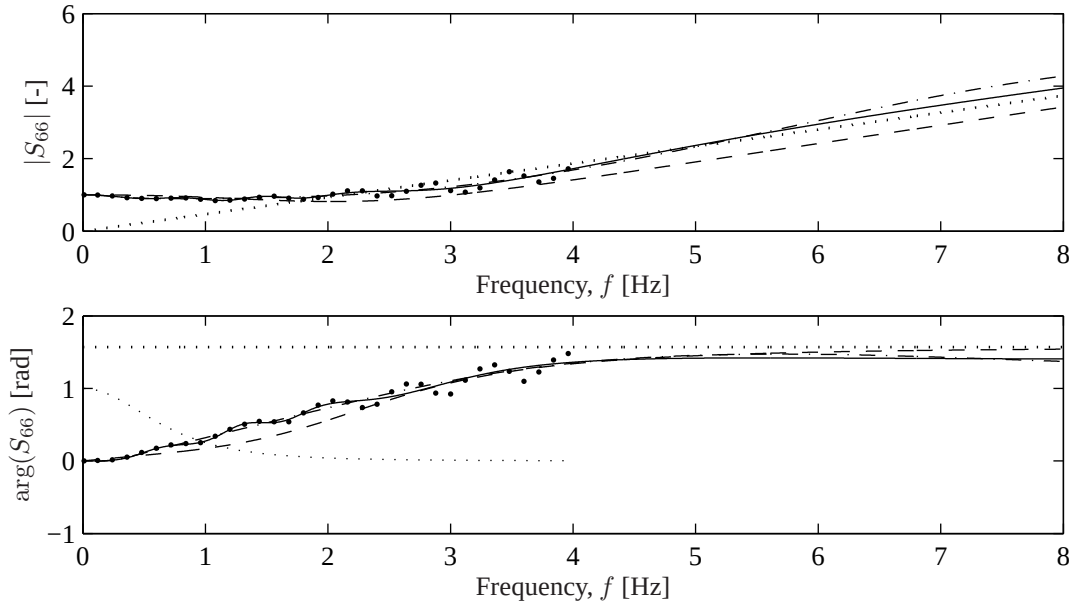

Figure 16: Dynamic stiffness coefficient, S_{66}, obtained by the domain-transformation model (the large dots) and lumped-parameter models with $M = 2$ (– –), $M = 6$ (– · – ·), and $M = 10$ (——). The thin dotted line (·····) indicates the weight function w (not in radians), and the thick dotted line (·····) indicates the high-frequency solution, i.e. the singular part of S_{66}.

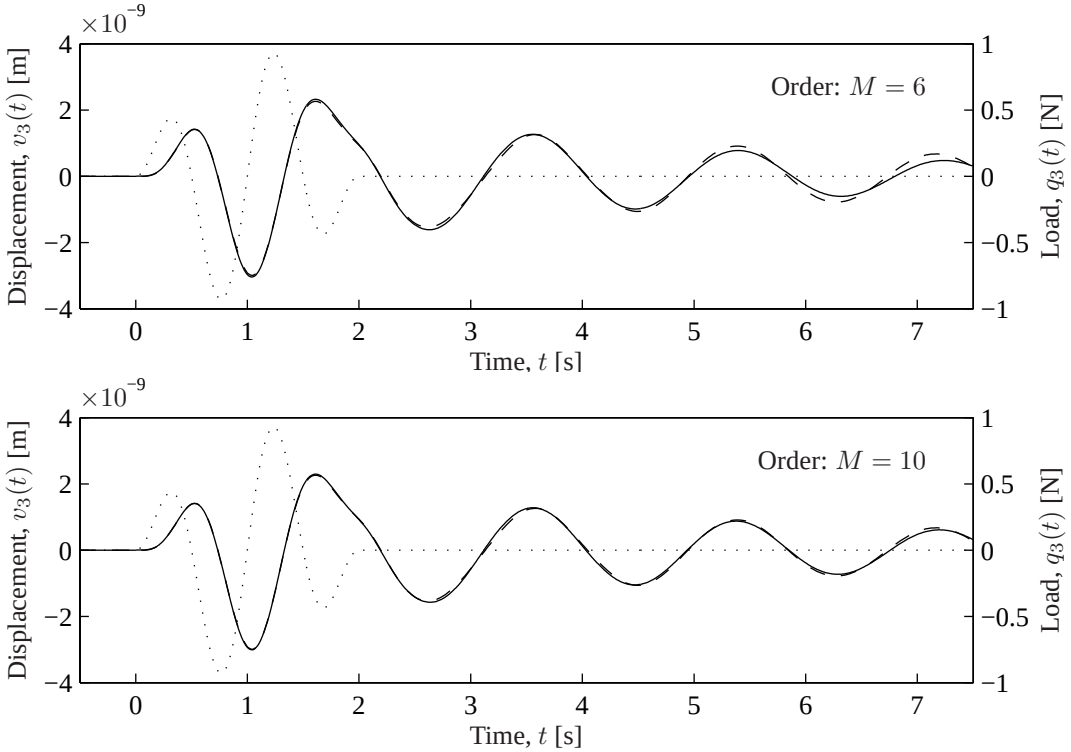

Figure 17: Response $v_3(t)$ obtained by inverse Fourier transformation (– –) and lumped-parameter model (——). The dots (·····) indicate the load time history.

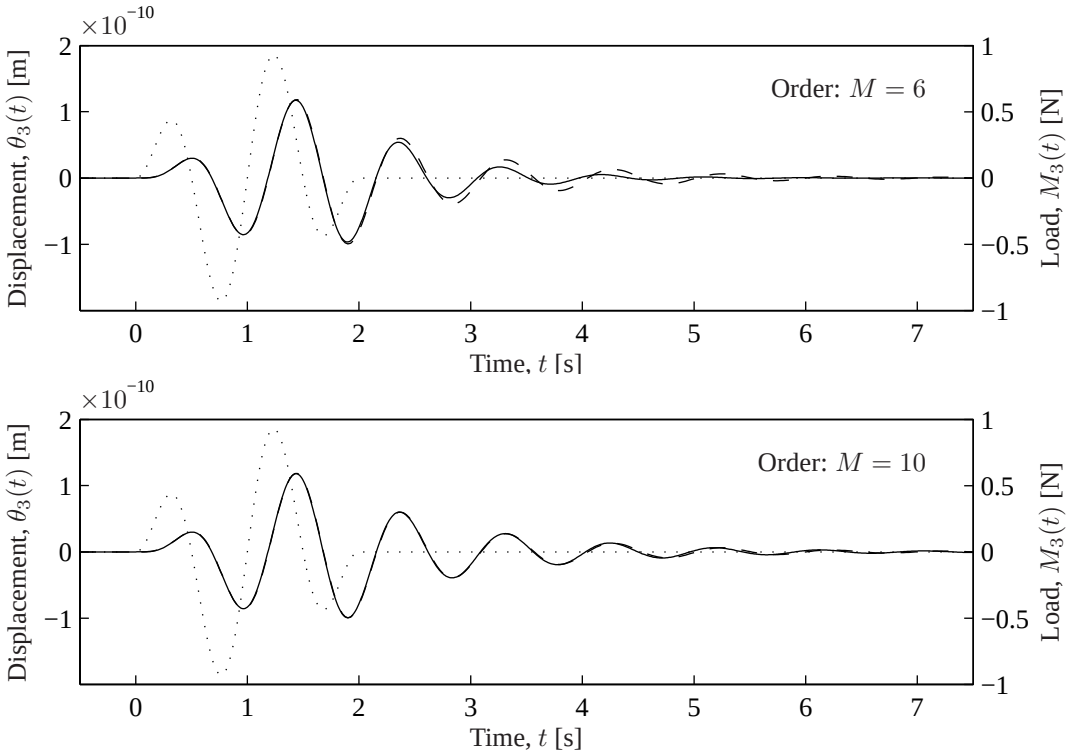

Figure 18: Response $\theta_3(t)$ obtained by inverse Fourier transformation (– –) and lumped-parameter model (——). The dots (·····) indicate the load time history.

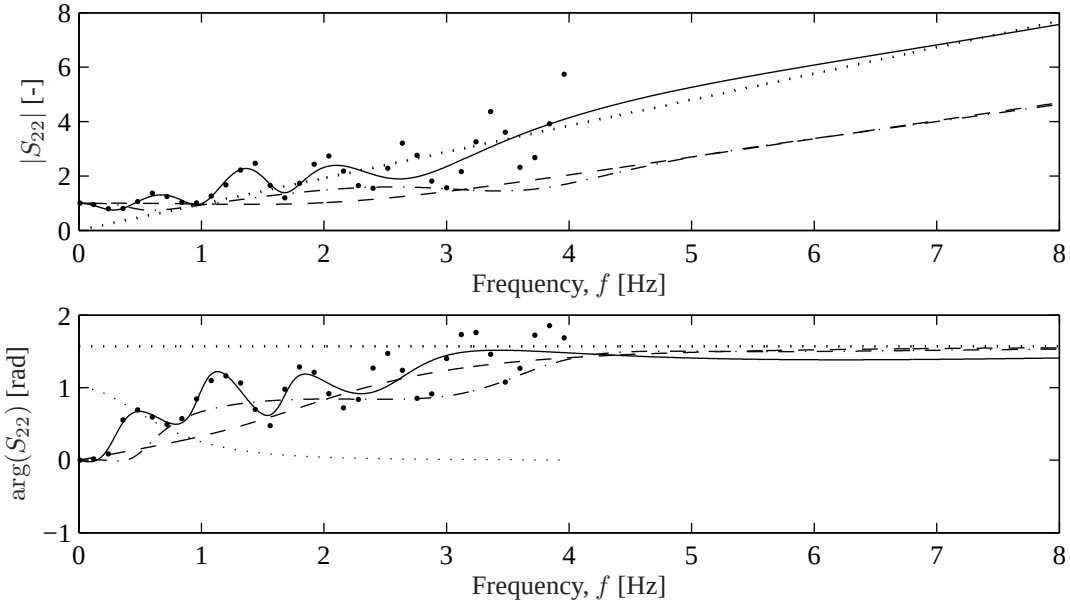

Figure 19: Dynamic stiffness coefficient, S_{22}, obtained by the domain-transformation model (the large dots) and lumped-parameter models with $M = 2$ (– –), $M = 6$ (– · – ·), and $M = 10$ (——). The thin dotted line (·····) indicates the weight function w (not in radians), and the thick dotted line (·····) indicates the high-frequency solution, i.e. the singular part of S_{22}.

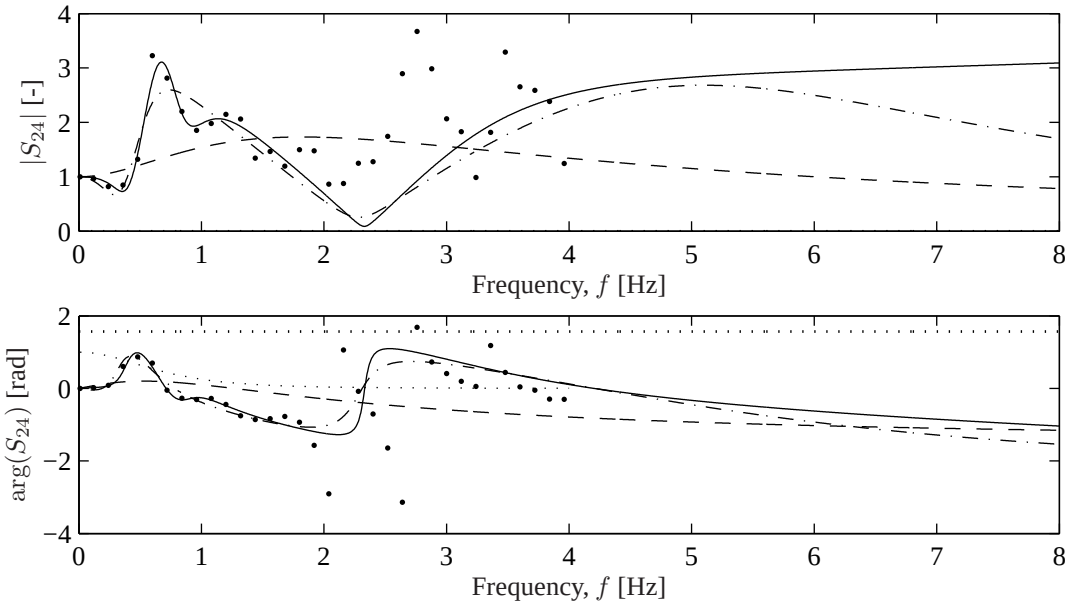

Figure 20: Dynamic stiffness coefficient, S_{24}, obtained by the domain-transformation model (the large dots) and lumped-parameter models with $M = 2$ (– –), $M = 6$ (– · – ·), and $M = 10$ (——). The thin dotted line (·····) indicates the weight function w (not in radians), and the thick dotted line (·····) indicates the high-frequency solution, i.e. the singular part of S_{24}.

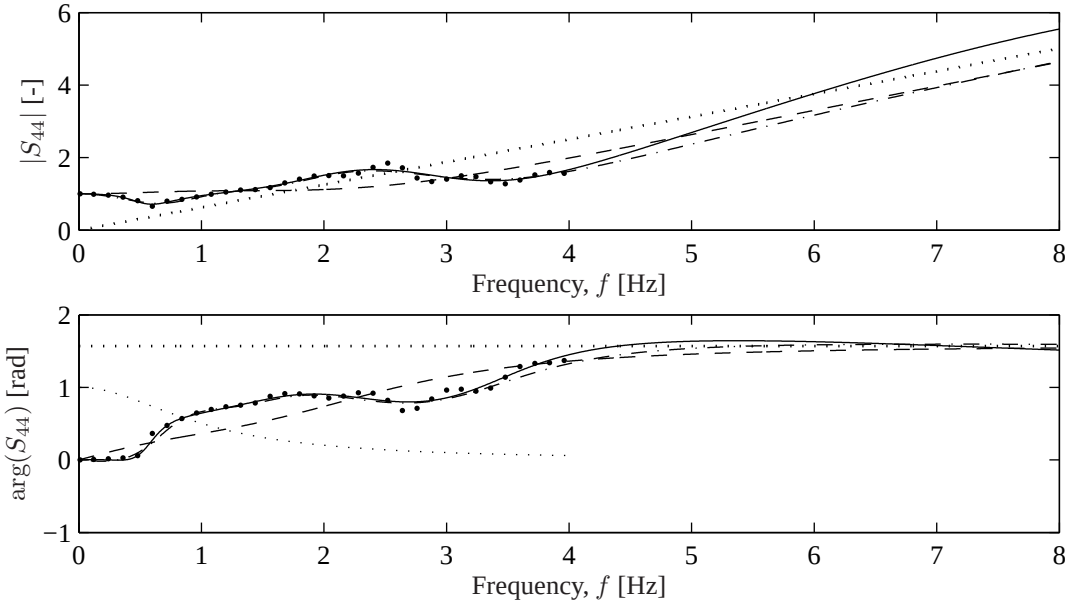

Figure 21: Dynamic stiffness coefficient, S_{44}, obtained by the domain-transformation model (the large dots) and lumped-parameter models with $M = 2$ (– –), $M = 6$ (– · – ·), and $M = 10$ (——). The thin dotted line (·····) indicates the weight function w (not in radians), and the thick dotted line (·····) indicates the high-frequency solution, i.e. the singular part of S_{44}.

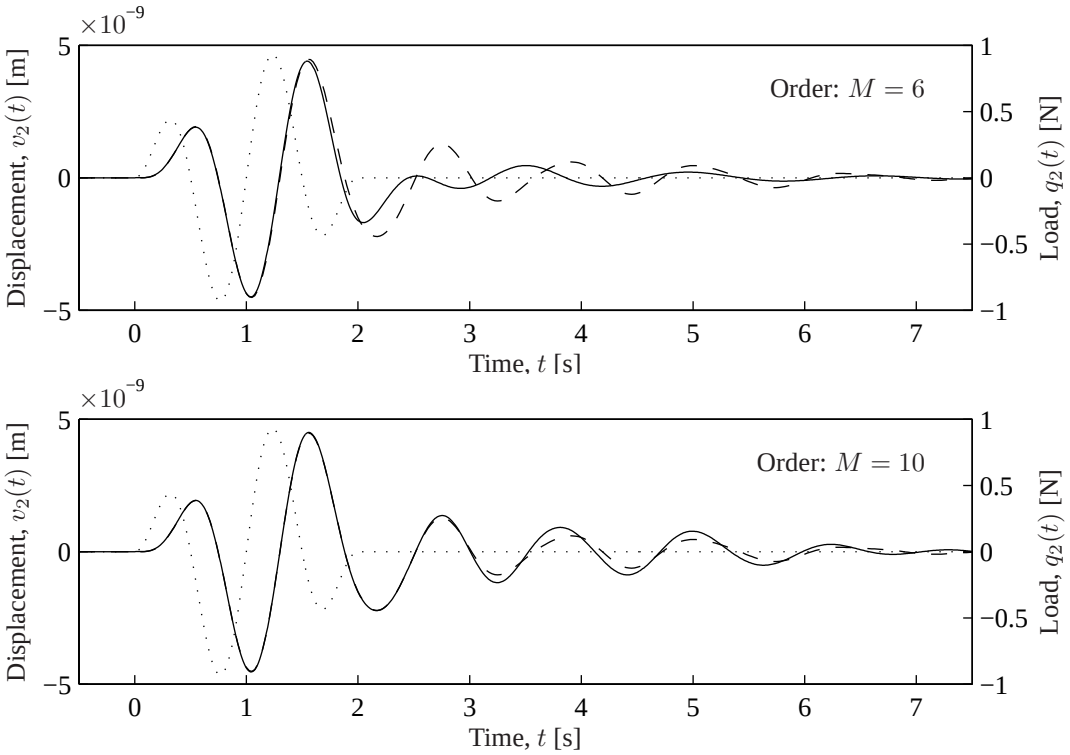

Figure 22: Response $v_2(t)$ obtained by inverse Fourier transformation (– –) and lumped-parameter model (——). The dots (·····) indicate the load time history.

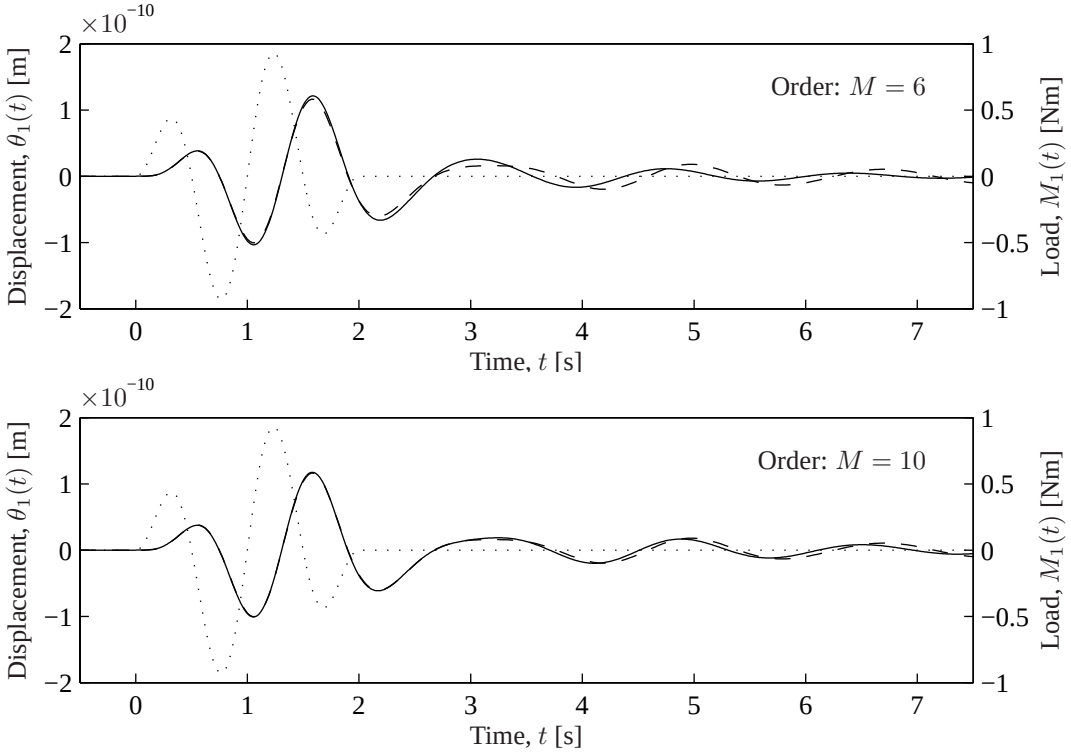

Figure 23: Response $\theta_1(t)$ obtained by inverse Fourier transformation (– –) and lumped-parameter model (——). The dots (·····) indicate the load time history.

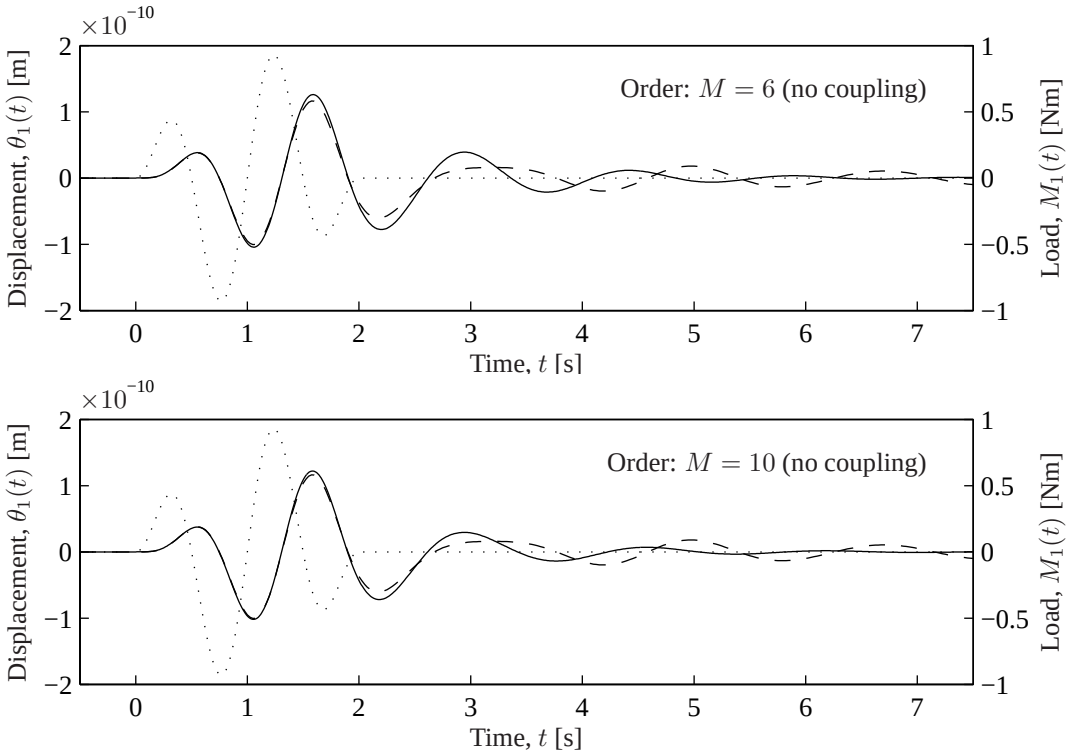

Figure 24: Response $\theta_1(t)$ obtained by inverse Fourier transformation (– –) and lumped-parameter model (——). The dots (·····) indicate the load time history.

Finally, in Fig. 24 the results are given for the alternative LPM, in which the coupling between sliding and rocking has been neglected. It is observed that the maximum response occurring during loading is predicted with almost the same accuracy as by the model in which the coupling is accounted for. However, the geometrical damping is badly described with regard to the decrease in magnitude and, in particular, the phase of the response during the free vibration.

6 Conclusion

The paper presents a study of lumped-parameter models applied to time-domain analysis of hexagonal footings on homogeneous or layered soil. Firstly, a short introduction is given to the domain-transformation method that has been utilised for the construction of a frequency-domain solution. Secondly, an algorithm is presented that brings the solution to the time domain by fitting a lumped-parameter model (LPM) to the impedance functions for the footing.

For the footing on the homogeneous soil it is found that an LPM with two internal degrees of freedom for the vertical and each of the sliding and rocking degrees of freedom provides a model of great accuracy. This corresponds to fourth-order rational approximations for each of the response spectra obtained by the domain-transformation method. Little improvement is gained by including an additional internal degree of freedom. Furthermore, it is concluded that little accuracy is lost by neglecting the coupling between the sliding and rocking motion. However, a sixth-order model is necessary in order to get an accurate representation of the torsional impedance.

Next, a footing on a stratified ground is analysed. Here the response cannot be predicted with low order models, and an LPM with 3–5 internal degrees of freedom is necessary for each nonzero term in the impedance matrix, i.e. rational approximations of the order 6–10 are required. In particular, it is noted that the impedance term providing the coupling between sliding and rocking is not easily fitted by an LPM of low order, i.e. orders below six. The maximum response is well predicted without the coupling term; however, if the coupling is not accounted for, the geometrical damping is poorly described. This may lead to erroneous conclusions regarding the fatigue lifespan of structures exposed to multiple transient dynamic loads, e.g. offshore wind turbines.

References

[1] J.E. Luco and R.A. Westmann, “Dynamic Response of Circular Footings”, Journal of Engineering Mechanics, ASCE, 97(5), 1381–1395, 1971.

[2] A.S. Veletsos and V.V. Damodaran Nair, “Torsional Vibration of Viscoelastic Foundations”, Journal of Geotechnical Engineering Division, ASCE, 100, 225–246, 1974.

[3] M. Novak and K. Sachs, “Torsional and Coupled Vibrations of Embedded Footings”, Earthquake Engineering and Structural Dynamics, 2, 11–33, 1973.

[4] J. Avilés and L.E. Pérez-Rocha, “A Simplified Procedure for Torsional Impedance Functions of Embedded Foundations in a Soil Layer”, Computers and Geotechnics, 19(2), 97–115, 1996.

[5] S. Krenk and H. Schmidt, “Vibration of an Elastic Circular Plate on an Elastic Half Space—A Direct Approach”, Journal of Applied Mechanics, 48, 161–168, 1981.

[6] Y. Yong, Ruichong Zhang and J. Yu, “Motion of Foundation on a Layered Soil Medium—I. Impedance Characteristics”, Soil Dynamics and Earthquake Engineering, 16, 295–306, 1997.

[7] A.S. Veletsos and Y.T. Wei, “Lateral and Rocking Vibration of Footings”, Journal of Soil Mechanics and Foundation Engineering Division, ASCE, 97, 1227–1248, 1971.

[8] J.E. Luco, “Vibrations of a Rigid Disk on a Layered Viscoelastic Medium”, Nuclear Engineering and Design, 36(3), 325–240, 1976.

[9] H.L. Wong and J.E. Luco, “Tables of Impedance Functions for Square Foundations on Layered Media”, Soil Dynamics and Earthquake Engineering, 4(2), 64–81, 1985.

[10] C. Vrettos, “Vertical and Rocking Impedances for Rigid Rectangular Foundations on Soils with Bounded Non-homogeneity”, Earthquake Engineering and Structural Dynamics, 28, 1525–1540, 1999.

[11] S. Bu and C.H. Lin, “Coupled Horizontal–Rocking Impedance Functions for Embedded Square Foundations at High Frequency Factors”, Journal of Earthquake Engineering, 3(4), 561–587, 1999.

[12] X. Sheng, “Ground Vibrations Generated from Trains”, PhD thesis, Institute of Sound and Vibration Research, University of Southampton, United Kingdom, 2001.

[13] L. Andersen, “Wave Propagation in Inifinite Structures and Media”, PhD thesis, Department of Civil Engineering, Aalborg University, Denmark, 2002.

[14] X. Sheng, C.J.C. Jones and M. Petyt, “Ground Vibration Generated by a Harmonic Load Acting on a Railway Track”, Journal of Sound and Vibration, 225(1), 3–28, 1999.

[15] L. Auersch, “Wave Propagation in Layered Soils: Theoretical Solution in Wavenumber Domain and Experimental Results of Hammer and Railway Traffic Excitation”, Journal of Sound and Vibration, 173(2), 233–264, 1994.

[16] L. Andersen and J. Clausen. “Impedance of Surface Footings on Layered Ground”, in “Proceedings of The Tenth International Conference on Civil, Structural and Environmental Engineering Computing”, B.H.V. Topping (Editor), Stirling, United Kingdom, 2005, Civil-Comp Press, Paper 255.

[17] J.P. Wolf, “Foundation Vibration Analysis Using Simple Physical Models”, Prentice-Hall, Englewood Cliffs, NJ, 1994.

[18] M. Liingaard, “DCE Thesis 3: Dynamic Behaviour of Suction Caissons”, PhD thesis, Department of Civil Engineering, Aalborg University, Denmark, 2006.

[19] K. Schittkowski, “NLPQL: A Fortran Subroutine for Solving Constrained Nonlinear Programming Problems”, Annals of Operations Research, 5, 485–500, 1985/86.

[20] N.M. Newmark, “A Method of Computation for Structural Dynamics”, ASCE Journal of the Engineering Mechanics Division, 85(EM3), 67–94, 1959.

ISSN 1901-7278
DCE Technical Memorandum No. 5